Towards the understanding of fully-heavy tetraquark states from various models

Chengrong Deng[1,*] Hong Chen,[1,†] and Jialun Ping[2,‡]

[1]*Department of Physics, Southwest University, Chongqing 400715, China*
[2]*Department of Physics, Nanjing Normal University, Nanjing 210097, China*

We use a color-magnetic interaction model (CMIM), a traditional constituent quark model and a multiquark color flux-tube model to systematically investigate the properties of the states $[Q_1Q_2][\bar{Q}_3\bar{Q}_4]$ ($Q = c$, b). The dynamical investigation indicates that the CMIM can not completely absorb QCD dynamical effects through the effective constituent quark mass and overestimates the color-magnetic interaction in the states under the assumption of the same spatial configurations. The Coulomb interaction plays a critical role in the dynamical model calculations on the heavy hadrons, which induces the fact that none of bound states $[Q_1Q_2][\bar{Q}_3\bar{Q}_4]$ can be found in the dynamical models. The color configuration $[[Q_1Q_2]_{\mathbf{6}_c}[\bar{Q}_3\bar{Q}_4]_{\bar{\mathbf{6}}_c}]_{\mathbf{1}}$ should be taken seriously in the ground states due to the strong Coulomb attraction between the $[Q_1Q_2]_{\mathbf{6}_c}$ and $[\bar{Q}_3\bar{Q}_4]_{\bar{\mathbf{6}}_c}$. The color configuration $[[Q_1Q_2]_{\bar{\mathbf{3}}_c}[\bar{Q}_2\bar{Q}_4]_{\mathbf{3}_c}]_{\mathbf{1}}$ is absolutely dominant in the excited states because of the strong Coulomb attraction within the $[Q_1Q_2]_{\bar{\mathbf{3}}_c}$ and $[\bar{Q}_2\bar{Q}_4]_{\mathbf{3}_c}$. The J/Ψ-pair resonances recently observed by LHCb are difficult to be accommodated in the CMIM. The broad structure ranging from 6.2 to 6.8 GeV can be described as the ground tetraquark state $[cc][\bar{c}\bar{c}]$ in the various dynamical models. The narrow structure $X(6900)$ can be identified as the excited state $[cc][\bar{c}\bar{c}]$ with $L = 1$ ($L = 2$) in the constituent quark model (color flux-tube model).

I. INTRODUCTION

The dynamics in the fully-heavy tetraquark states is very simple, which only includes perturbative one gluon exchange (OGE) interaction and nonperturbative color confinement potential. They can provide a unique environment to examine the non-relativistic quark model with quantum chromodynamics (QCD) effective potentials if they do exist. The question of whether there exist such states has been debated for more than 40 years [1], which received much attention from the different theoretical frameworks, such as the nonrelativistic quark models [2–5], the color-magnetic interaction model (CMIM) [6–9], the QCD sum rules [10], the Bethe-Salpeter equation [11], MIT bag model [12], the lattice QCD [13] etc. The conclusions were model dependent. Taking the state $bb\bar{b}\bar{b}$ as an example, it can exist as a stable state against strong interaction in the spin-spin interaction model [14], while it

*crdeng@swu.edu.cn
†chenh@swu.edu.cn
‡jlping@njnu.edu.cn

is not stable in the string model [15]. Due to these controversial issues, relevant experimental studies are significant to understand their properties.

On the experimental side, the ATLAS, CMS, and LHCb collaborations have measured the cross section for double charmonium production [16]. In 2018, the LHCb collaboration investigated the $\Upsilon\mu^+\mu^-$ invariant-mass distribution to search for a possible fully-heavy tetraquark state $bb\bar{b}\bar{b}$, and observed no significant excess [17]. Very recently, the LHCb Collaboration researched the invariant mass spectrum of J/Ψ pairs using proton-proton collision data at center-of-mass energies of $\sqrt{s} = 7$, 8 and 13 TeV [18]. They found a broad structure ranging from 6.2 to 6.8 GeV and a narrow structure around 6.9 GeV. The narrow structure, denoted as $X(6900)$, is assumed as a resonance with the Breit-Wigner line shape. The structures are the first to be made up of four heavy quarks of the same type, which provides an extreme and yet theoretically fairly simple case to explore the strong interaction and to test models that can be used to explain the nature of ordinary hadrons.

The structures have revitalized the investigations of multiquark resonances made of heavy quarks and heavy antiquarks. Many theoretical investigations have been devoted to interpret the properties of the structures [19,20]. However, their properties and spin-parity quantum

numbers are not completely clear so far. It is therefore necessary to carry out a dynamical investigation on the fully-heavy tetraquark states from various theoretical frameworks, which is propitious to identify the properties of the structures and to broaden our horizons of the fully-heavy exotic hadrons.

In this work, we prepare to make a systematical research on the states $[Q_1Q_2][\bar{Q}_3\bar{Q}_4]$ from the perspective of the phenomenological models, including the color-magnetic interaction model, traditional constituent quark model and multiquark color flux-tube model. The CMIMs have various versions [21], the model with reference mass scale is employed here [22]. The traditional constituent quark model includes the OGE interaction and two-body confinement potential proportional to color charge. The multiquark color flux-tube model based on the lattice QCD color flux-tube picture and the traditional quark model has been developed, which contains a multibody confinement potential instead of two-body one. The model was recently applied to systematically investigate the states $[cs][\bar{c}\bar{s}]$ [23]. Furthermore, the conclusions of other phenomenological models are involved to make a comprehensive understanding on the fully-heavy tetraquark states.

This paper is organized as follows. After the introduction section, the descriptions of three models are given in Sec. II. The wave function of the states $[Q_1Q_2][\bar{Q}_3\bar{Q}_4]$ is shown in Sec. III. The numerical results and discussions are presented in Sec. IV. A brief summary is listed in the last section.

II. THREE MODELS

QCD has been widely accepted as the fundamental theory to describe the strong interaction among quarks and gluons and hadron structure, in which quarks and antiquarks are in the fundamental representation of the non-Abelian SU(3) color gauge group while gluons belong to the adjoint representation. At the hadronic scale, QCD is highly nonperturbative due to the complicated infrared behavior of the non-Abelian SU(3) gauge group. Unfortunately, calculating the properties of hadrons analytically from the QCD Lagrangian has proven to be a very difficult task in this strongly coupled nonlinear theory. In the long term, lattice QCD, which formulates the theory on a discrete space-time lattice, is the most promising technique. One can calculate hadron properties from the first principles by constructing interpolating fields with the quantum numbers of physical hadrons and evaluating their correlations on the lattice. Although a great deal of progress has been made, it has been slow since these calculations take enormous amounts of computer time. A less rigorous approach, which has proven to be quite useful and reasonably successful, has been to use QCD-motivated phenomenological models to describe hadron properties.

A. Color-magnetic interaction model

The original form of the color-magnetic interaction between the particles i and j can be expressed as follows,

$$V_{ij}^{\mathrm{cm}} = -\frac{\pi\alpha_s\delta(\mathbf{r}_{ij})\lambda_i^c \cdot \lambda_j^c\boldsymbol{\sigma}_i \cdot \boldsymbol{\sigma}_j}{6m_im_j}, \qquad (1)$$

it is the spin-dependent part of the OGE interaction V_{ij}^{oge} [24],

$$V_{ij}^{\mathrm{oge}} = \frac{\alpha_s}{4}\lambda_i^c \cdot \lambda_j^c\left(\frac{1}{r_{ij}} - \frac{2\pi\delta(\mathbf{r}_{ij})\boldsymbol{\sigma}_i \cdot \boldsymbol{\sigma}_j}{3m_im_j}\right), \qquad (2)$$

m_i and $\mathbf{r}_i$ are the effective mass and position of the particle i, respectively. $\mathbf{r}_{ij} = \mathbf{r}_i - \mathbf{r}_j$ and $r_{ij} = |\mathbf{r}_i - \mathbf{r}_j|$. λ^c and σ represent the Gell-Mann matrices and the Pauli matrices, respectively. α_s is a running quark-gluon coupling constant in the perturbative QCD. More details will be given in the following introduction of the constituent quark model.

With the exception of the spin-color factor $\lambda_i^c \cdot \lambda_j^c\boldsymbol{\sigma}_i \cdot \boldsymbol{\sigma}_j$, the other part of the color-magnetic interaction can be denoted as

$$C_{ij} = \frac{\pi\alpha_s\delta(\mathbf{r}_{ij})}{6m_im_j}, \qquad (3)$$

It incorporates the effects from the spatial configuration and effective quark masses and describes the effective coupling constant between the particles i and j. For n-body ground states, the total color-magnetic interaction can be written as

$$H_{\mathrm{cm}}^n = -\sum_{i<j}^n C_{ij}\lambda_i^c \cdot \lambda_j^c\boldsymbol{\sigma}_i \cdot \boldsymbol{\sigma}_j, \qquad (4)$$

It leads to the mass splitting among different color-spin configurations. In the conventional mesons and baryons, the color factors are frozen because they are constant, $\langle\lambda_i^c \cdot \lambda_j^c\rangle = -\frac{8}{3}$ for baryons and $\langle\lambda_i^c \cdot \lambda_j^c\rangle = -\frac{16}{3}$ for mesons. The calculation of color-magnetic interaction therefore reduces to the simple algebra of the spin-spin operator $\boldsymbol{\sigma}_i \cdot \boldsymbol{\sigma}_j$. In the case of the tetraquark state with diquark-antiquark configuration, the values $\langle\boldsymbol{\sigma}_i \cdot \boldsymbol{\sigma}_j\rangle$ and $\langle\lambda_i^c \cdot \lambda_j^c\rangle$ can be calculated according to the symmetry properties of the tetraquark wave function [25]. In addition, they can also be calculated according to the definition of spin and color operators with our computer programs. A multiquark state with given total quantum numbers in general consists of several channels with different intermediate quantum numbers. Using the values $\langle\boldsymbol{\sigma}_i \cdot \boldsymbol{\sigma}_j\rangle$, $\langle\lambda_i^c \cdot \lambda_j^c\rangle$ and C_{ij}, the color-magnetic interaction matrices can be obtained [22]. Finally, the color-magnetic interaction energies of the multiquark states can be achieved after we diagonalize the numerical color-magnetic interaction matrices.

The effective quark masses should also be involved in the CMIM Hamiltonian, which is assumed to be able to absorb other various QCD dynamic effects, such as kinetic energy, Coulomb interaction and confinement potential. Therefore, the mass formula of n-body ground states in the CMIM reads

$$M = \sum_{i=1}^{n} m_i + \langle H_{\mathrm{cm}}^n \rangle. \qquad (5)$$

In principle, the values of m_i and C_{ij} should be different in the various hadron environment. However, it is difficult to exactly obtain the effect from the spatial configuration because of no knowing the spatial wave function. Therefore, the CMIM assumes that two pairs of interactional particles with the same quark content share the same size in the generalization from conventional hadrons to multiquark states. For the simplicity and model universality, the values of m_i and C_{ij} are usually extracted from the masses of conventional hadrons and then extended to multiquark states [21]. This mechanism has been applied to investigate the properties of the well-known H particle and heavy pentaquark state $qqqq\bar{Q}$ [26,27]. Recently, the mechanism was also widely utilized to study the natures of some new hadrons [28].

The mass formula generally overestimate the mass of conventional hadrons [21], especially the mesons. In the case of various multiquark states, the obtained masses with this mass formula are also the largest values [28]. The reason of the overestimation on the mass is probably from the fact that the dynamical effects cannot be simply absorbed into the effective quark masses. In order to reduce the uncertainties and obtain more appropriate estimations, an alternative mass formula has been developed to avoid generally overestimated masses [22],

$$M = M_{\mathrm{ref}} - \langle H_{\mathrm{cm}}^n \rangle_{\mathrm{ref}} + \langle H_{\mathrm{cm}}^n \rangle. \qquad (6)$$

M_{ref} and $\langle H_{\mathrm{cm}}^n \rangle_{\mathrm{ref}}$ are the physical mass of the reference system and its corresponding color-magnetic interaction energy, respectively. A multiquark (tetraquark) state is generally related to a reference hadron-hadron (meson-meson) system whose quark content and quantum numbers are the same as those of the considered multiquark state. This mass formula can evade the problem of using extracted quark masses from conventional hadrons in the multiquark states [29]. Meanwhile, it can phenomenologically compensate the part of missed attraction between quark components in the multiquark states.

In the present work, we focus on the CMIM results of the states $[Q_1 Q_2][\bar{Q}_3 \bar{Q}_4]$ obtained from the reference mass formula. The parameters C_{ij} related to ground heavy-meson states are taken from Ref. [21], some of which are used here are listed in Table I.

TABLE I. Parameters C_{ij} for the ground heavy-meson states, unit in MeV.

C_{ij}	$C_{c\bar{q}}$	$C_{c\bar{s}}$	$C_{\bar{c}c}$	$C_{\bar{b}q}$	$C_{\bar{b}s}$	$C_{\bar{b}b}$	$C_{\bar{b}c}$
Value	6.6	6.7	5.3	2.1	2.3	2.9	3.3

According to the alternative mass formula, one can define the binding energy of a tetraquark state as

$$\Delta E = M - M_{\mathrm{ref}} = \langle H_{\mathrm{cm}}^n \rangle - \langle H_{\mathrm{cm}}^n \rangle_{\mathrm{ref}} \qquad (7)$$

to identify whether or not the state is stable against strong interaction. If $\Delta E \geq 0$, the state can fall apart into the two mesons through quark rearrangement. If $\Delta E < 0$, the strong decay into the two mesons is forbidden and therefore the decay must be weak or electromagnetic interaction. In fact, such an estimation method had been applied to search for stable multiquark states many years ago [30].

B. Constituent quark model

Constituent quark model (CQM) is formulated under the assumption that hadrons are color singlet nonrelativistic bound states of constituent quarks with effective masses and interactions. One expects that the model dynamics is governed by QCD. The perturbative effect of QCD is well described by the OGE interaction, which is a standard color Fermi-Breit interaction given by the Lagrangian

$$\mathcal{L}_{\mathrm{oge}} = i\sqrt{4\pi}\alpha_s \bar{q}\gamma_\mu G^\mu \lambda^c q \qquad (8)$$

where G^μ is the gluon field and q is the quark fields, both of which carry the color charge. γ_μ is the Dirac matrix. From the nonrelativistic reduction of the OGE diagram in QCD for pointlike quarks one gets

$$V_{ij}^{\mathrm{oge}} = \frac{\alpha_s}{4}\lambda_i^c \cdot \lambda_j^c \left(\frac{1}{r_{ij}} - \frac{2\pi\delta(\mathbf{r}_{ij})\boldsymbol{\sigma}_i \cdot \boldsymbol{\sigma}_j}{3m_i m_j} \right). \qquad (9)$$

Dirac $\delta(\mathbf{r}_{ij})$ function comes out in the deduction of the interaction between pointlike quarks, when not treated perturbatively, which leads to collapse [31]. Therefore, the $\delta(\mathbf{r}_{ij})$ function can be regularized in the form [32]

$$\delta(\mathbf{r}_{ij}) \rightarrow \frac{1}{4\pi r_{ij} r_0^2(\mu_{ij})} e^{-r_{ij}/r_0(\mu_{ij})}, \qquad (10)$$

where $r_0(\mu_{ij}) = \hat{r}_0/\mu_{ij}$, $\hat{r}_0$ is an adjustable model parameter. This regularization is justified based on the finite size of the constituent quarks and should be therefore flavor dependent [33].

The quark-gluon coupling constant α_s in the perturbative QCD reads [34]

$$\alpha_s(\mu^2) = \frac{1}{\beta_0 \ln \frac{\mu^2}{\Lambda^2}}. \tag{11}$$

In the present work, we use an effective scale-dependent form given by

$$\alpha_s(\mu_{ij}^2) = \frac{\alpha_0}{\ln \frac{\mu_{ij}^2}{\Lambda_0^2}}, \tag{12}$$

where μ_{ij} is the reduced mass of two interacting particles, namely $\mu_{ij} = \frac{m_i m_j}{m_i + m_j}$. Λ_0 and α_0 are adjustable model parameters.

Besides the OGE interaction, CQM model imitating QCD should also incorporate nonperturbative effect, color confinement, which takes into account the fact that the only observed hadrons are color singlets. Color confinement plays an essential role in the low energy hadron physics. However, it is still impossible to derive color confinement analytically from its QCD Lagrangian so far. From the perspective of phenomenological models, quark confinement potential should only emerge from a model in which the interaction depends on color charges. In addition, the coupling between color charges increases with increasing separation in QCD. Quark confinement potential in the CQM can be manmade based on the two ingredients, which is defined as the sum of two-body interactions proportional to the color charges and r_{ij}^2 [35],

$$V^{con} = -a_c \sum_{i<j}^n \lambda_i^c \cdot \lambda_j^c r_{ij}^2, \tag{13}$$

where a_c is an adjustable model parameter.

To sum up, the completely Hamiltonian of the CQM for the heavy mesons and fully-heavy tetraquark states can be presented as

$$H_n = \sum_{i=1}^n \left(m_i + \frac{\mathbf{p}_i^2}{2m_i} \right) - T_c + \sum_{i<j}^n V_{ij}^{oge} + V^{con}. \tag{14}$$

T_c is the center-of-mass kinetic energy of the states and should be deducted; $\mathbf{p}_i$ is the momentum of the ith quark or antiquark.

The model can automatically prevent overall color singlet multiquark states disintegrating into several color subsystems by means of color confinement with an appropriate $SU_c(3)$ Casimir constant [36]. The model also allows a multiquark system disintegrating into color-singlet clusters, and it leads to interacting potentials within mesonlike $q\bar{q}$ and baryonlike qqq subsystems in accord with the empirically known potentials [36]. However, the model is known to be flawed phenomenologically because it leads to power law van der Waals forces between color-singlet hadrons. In addition, it also leads to

TABLE II. Model parameters, quark mass and Λ_0 unit in MeV, a_c unit in MeV $\cdot$ fm^{-2}, r_0 unit in MeV $\cdot$ fm^{-2} and α_0 is dimensionless.

Para.	$m_{u,d}$	m_s	m_c	m_b	a_c	α_0	Λ_0	r_0
Valu.	313	494	1664	5006	−150	4.25	40.85	119.3

anticonfinement for symmetrical color structure in the multiquark system [37].

In order to avoid the misjudgement of the behavior of model dynamics due to inaccurate numerical results, a high precision computational method is therefore indispensable. The Gaussian expansion method (GEM) [38], which has been proven to be a rather powerful numerical method to solve few-body problem in nuclear physics, is therefore widely used to study multibody systems. According to the GEM, the relative motion wave function between the quark and antiquark in the heavy mesons can be written as

$$\phi_{lm}^G(\mathbf{r}) = \sum_{n=1}^{n_{max}} c_n N_{nl} r^l e^{-\nu_n r^2} Y_{lm}(\hat{\mathbf{r}}). \tag{15}$$

Gaussian size parameters are taken as geometric progression

$$\nu_n = \frac{1}{r_n^2}, \qquad r_n = r_1 a^{n-1}, \qquad a = \left(\frac{r_{n_{max}}}{r_1} \right)^{\frac{1}{n_{max}-1}} \tag{16}$$

N_{nl} is normalized coefficient and c_n is a variation coefficient determined by the model dynamics. More details about the GEM can be found in Ref. [38]. With $r_1 = 0.2$ fm, $r_{n_{max}} = 2.0$ fm and $n_{max} = 7$, the converged numerical results can be achieved in the present work.

The mass of ud quark is taken to be one third of that of nucleon, other adjustable model parameters in Table II can be determined by solving two-body Schrödinger equation with the trial wave function Eq. (13) to fit the ground heavy meson states, which is listed in Table III. At the same time, we also give the average values of various parts of the CQM Hamiltonian. $\langle E_k \rangle$, $\langle V^{con} \rangle$, $\langle V^{cm} \rangle$, and $\langle V^{clb} \rangle$ represent the average values of kinetic energy, confinement potential, color-magnetic interaction and Coulomb interaction, respectively. It can been found from Table III that the Coulomb interaction provides an extremely strong short-range attraction, which is the main reason why a quark and an antiquark can form a bound state in the CQM.

In the CMIM, the matrix elements $\langle \sigma_i \cdot \sigma_j \rangle = -3$ and 1 for spin $S = 0$ and spin $S = 1$, respectively. Under the assumption of the same spatial configuration, the color-magnetic interaction gives an energy ratio $3:1$ between spin $S = 0$ and $S = 1$ mesons with the same quark content in the CMIM, such as D and D^*. In the dynamical calculation of the CQM, the same flavor mesons with different spin do not share the same spatial configuration

TABLE III. Ground state heavy-meson spectra and the average values of various parts of the Hamiltonian in MeV and the average distance in fm.

States	PDG	E_2	$\langle E_k \rangle$	$\langle V^{con} \rangle$	$\langle V^{cm} \rangle$	$\langle V^{clb} \rangle$	$\langle r^2 \rangle^{\frac{1}{2}}$
$D^\pm$	1869	1886	737	200	-92	-937	0.50
D^*	2007	2000	633	226	27	-862	0.53
$D_s^\pm$	1969	1982	693	151	-105	-914	0.43
D_s^*	2112	2109	560	179	29	-816	0.47
η_c	2980	2965	679	75	-123	-995	0.31
J/Ψ	3097	3103	488	97	29	-838	0.35
B^0	5280	5261	664	197	-34	-885	0.50
B^*	5325	5305	623	207	11	-855	0.51
B_s^0	5366	5346	612	143	-42	-868	0.42
B_s^*	5416	5399	555	155	13	-824	0.44
B_c	6277	6244	644	54	-79	-1044	0.26
B_c^*	$\cdots$	6336	502	65	20	-921	0.29
η_b	9391	9376	740	24	-96	-1305	0.17
$\Upsilon(1S)$	9460	9486	560	30	24	-1140	0.19

because of their different dynamics, see the average distance $\langle r^2 \rangle^{\frac{1}{2}}$ in Table III. The ratio in the dynamical calculation is not strict 3:1 because of the same reason, which is between 3:1 and 4:1. It is therefore approximately reasonable to describe the mass splitting of mesons by the color magnetic interaction in the CMIM.

C. Multiquark color flux-tube model

Details of the multiquark color flux-tube model (MCFTM) based on traditional constituent quark models can be found in our previous paper [23]. Only prominent characteristics of the model are presented here. Within the framework of color flux-tube picture, the quark and antiquark in a meson are linked with a three-dimensional color flux tube, see Fig. 1. A two-body confinement potential can be written as

$$V^{con}_{min}(2) = K r_{ij}^2, \qquad (17)$$

where r_{ij} is distance between the quark and antiquark. The parameter K is the stiffnesses of a three-dimensional color flux tube and determined by fitting the heavy-meson spectra. Comparing with the confinement potential in the CQM, one can obtain $K = -a_c \langle \lambda_i^c \cdot \lambda_j^c \rangle = 800$ MeV fm^{-2}.
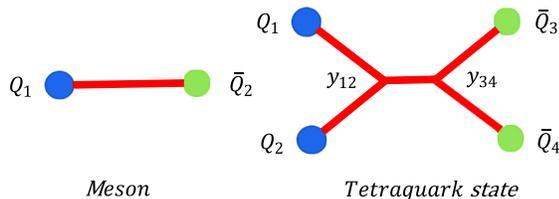
FIG. 1. Color flux-tube structures.

The fully-heavy tetraquark states favor the compact diquark-antiquark configuration rather than a loosely molecular states because of the lack of the light mesons exchange between two $Q\bar{Q}$ mesons. The color flux-tube structure of the diquark-antiquark configuration is given in Fig. 1. According to the double Y-shaped color flux-tube structure, a four-body quadratic confinement potential can be written as

$$V^{con}(4) = K[(\mathbf{r}_1 - \mathbf{y}_{12})^2 + (\mathbf{r}_2 - \mathbf{y}_{12})^2 + (\mathbf{r}_3 - \mathbf{y}_{34})^2 \\ + (\mathbf{r}_4 - \mathbf{y}_{34})^2 + \kappa_d (\mathbf{y}_{12} - \mathbf{y}_{34})^2], \qquad (18)$$

in which $\mathbf{r}_1$, $\mathbf{r}_2$, $\mathbf{r}_3$ and $\mathbf{r}_4$ represent the position of the Q_1, Q_2, $\bar{Q}_3$, and $\bar{Q}_4$, respectively. Two Y-shaped junctions $\mathbf{y}_{12}$ and $\mathbf{y}_{34}$ are variational parameters determined by taking the minimum of the confinement potential. The relative stiffness parameter κ_d is equal to $\frac{C_d}{C_3}$ [39], where C_d is the eigenvalue of the Casimir operator associated with the SU(3) color representation d at either end of the color flux tube, such as $C_3 = \frac{4}{3}$, $C_6 = \frac{10}{3}$, and $C_8 = 3$.

The minimum of the confinement potential $V^{con}_{min}(4)$ can be obtained by taking the variation of $V^{con}(4)$ with respect to $\mathbf{y}_{12}$ and $\mathbf{y}_{34}$, and it can be expressed as

$$V^{con}_{min}(4) = K \left(\mathbf{R}_1^2 + \mathbf{R}_2^2 + \frac{\kappa_d}{1 + \kappa_d} \mathbf{R}_3^2 \right). \qquad (19)$$

The canonical coordinates $\mathbf{R}_i$ have the following forms,

$$\mathbf{R}_1 = \frac{1}{\sqrt{2}} (\mathbf{r}_1 - \mathbf{r}_2), \qquad \mathbf{R}_2 = \frac{1}{\sqrt{2}} (\mathbf{r}_3 - \mathbf{r}_4),$$

$$\mathbf{R}_3 = \frac{1}{\sqrt{4}} (\mathbf{r}_1 + \mathbf{r}_2 - \mathbf{r}_3 - \mathbf{r}_4),$$

$$\mathbf{R}_4 = \frac{1}{\sqrt{4}} (\mathbf{r}_1 + \mathbf{r}_2 + \mathbf{r}_3 + \mathbf{r}_4). \qquad (20)$$

The use of $V^{con}_{min}(4)$ can be understood here as that the gluon field readjusts immediately to its minimal configuration.

The OGE interaction is also involved in the MCFTM, which is the same as that of the CQM. It is worth mentioning that the MCFTM is not a completely new model but the updated version of the traditional CQM based on the color flux-tube picture of hadrons in the lattice QCD. In fact, it merely modifies the two-body confinement potential into the multibody one to describe multiquark states with multibody interaction. The MCFTM reduces to the CQM in the mesons while the MCFTM can obtain different results from the CQM in the multiquark states.

III. WAVE FUNCTION

Numerical results of the states $[Q_1 Q_2][\bar{Q}_3 \bar{Q}_4]$ can be obtained by solving a four-body Schrödinger equation with their complete wave functions including all possible

flavor-spin-color-spatial channels that contribute to a given well defined parity, isospin, and total angular momentum. In the frame of center of mass, the wave functions of the states $[Q_1 Q_2][\bar{Q}_3 \bar{Q}_4]$ can be constructed as a sum of the following direct products of color χ_c, isospin η_i, spin χ_s, and spatial ϕ_{lm}^G terms

$$
\begin{aligned}
&\Phi_{IM_I JM_J}^{[Q_1 Q_2][\bar{Q}_3 \bar{Q}_4]} \\
&= \sum_\alpha \xi_\alpha [[[\phi_{l_a m_a}^G(\mathbf{r}) \chi_{s_a M_{s_a}}]_{J_a M_{J_a}}^{[Q_1 Q_2]} \\
&\quad \times \left[\phi_{l_b m_b}^G(\mathbf{R}) \chi_{s_b M_{s_b}}\right]_{J_b M_{J_b}}^{[\bar{Q}_3 \bar{Q}_4]}\right]_{J_{ab} M_{J_{ab}}} \phi_{l_{ab} m_{ab}}^G(\mathbf{X})\Big]_{JM_J} \\
&\quad \times \left[\eta_{i_a M_{i_a}}^{[Q_1 Q_2]} \eta_{i_b M_{i_b}}^{[\bar{Q}_3 \bar{Q}_4]}\right]_{IM_I} \left[\chi_{[c_a] W_{c_a}}^{[Q_1 Q_2]} \chi_{[c_b] W_{c_b}}^{[\bar{Q}_3 \bar{Q}_4]}\right]_{[C] W_C}.
\end{aligned} \tag{21}
$$

The subscripts a and b in the intermediate quantum numbers represent the $[Q_1 Q_2]$ and $[\bar{Q}_3 \bar{Q}_4]$, respectively. The summering index α stands for all possible flavor-spin-color-spatial intermediate quantum numbers. [ ]s denote Clebsh-Gordan coefficient coupling.

In the dynamical calculation, the relative spatial coordinates $\mathbf{r}$, $\mathbf{R}$, and $\mathbf{X}$ and center-of-mass $\mathbf{R}_c$ in the states $[Q_1 Q_2][\bar{Q}_3 \bar{Q}_4]$ can be defined as

$$
\begin{aligned}
\mathbf{r} &= \mathbf{r}_1 - \mathbf{r}_2, \qquad \mathbf{R} = \mathbf{r}_3 - \mathbf{r}_4, \\
\mathbf{X} &= \frac{m_1 \mathbf{r}_1 + m_2 \mathbf{r}_2}{m_1 + m_2} - \frac{m_3 \mathbf{r}_3 + m_4 \mathbf{r}_4}{m_3 + m_4}, \\
\mathbf{R}_c &= \frac{m_1 \mathbf{r}_1 + m_2 \mathbf{r}_2 + m_3 \mathbf{r}_3 + m_4 \mathbf{r}_4}{m_1 + m_2 + m_3 + m_4}.
\end{aligned} \tag{22}
$$

In the center-of-mass reference frame, the relative motion wave functions $\phi_{l_a m_a}^G(\mathbf{r})$, $\phi_{l_b m_b}^G(\mathbf{R})$, and $\phi_{l_{ab} m_{ab}}^G(\mathbf{X})$ can be expressed as the superposition of many different size Gaussian functions with well-defined quantum numbers, which share the exactly same form with that of the heavy mesons, to obtain accurate numerical results. For the sake of saving space, their explicit expressions are not presented here. The heavy quarks have isospin zero so they do not contribute to the total isospin. The flavor wave function is therefore symmetrical if Q_1 and Q_2 ($\bar{Q}_3$ and $\bar{Q}_4$) are identical particles.

The color representation of the $[\bar{Q}_3 \bar{Q}_4]$ ($[Q_1 Q_2]$) may be antisymmetrical $\mathbf{3}_c$ ($\bar{\mathbf{3}}_c$) or symmetrical $\bar{\mathbf{6}}_c$ ($\mathbf{6}_c$). Coupling the colorful $[Q_1 Q_2]$ and $[\bar{Q}_3 \bar{Q}_4]$ into an overall colorless state according to color coupling rule, we have two different coupling ways: $[[Q_1 Q_2]_{\bar{\mathbf{3}}_c} \otimes [\bar{Q}_3 \bar{Q}_4]_{\mathbf{3}_c}]_{\mathbf{1}}$ and $[[Q_1 Q_2]_{\mathbf{6}_c} \otimes [\bar{Q}_3 \bar{Q}_4]_{\bar{\mathbf{6}}_c}]_{\mathbf{1}}$. The spin of the $[Q_1 Q_2]$ is coupled to s_a and that of the $[\bar{Q}_3 \bar{Q}_4]$ is coupled to s_b. The total spin wave function of the state $[Q_1 Q_2][\bar{Q}_3 \bar{Q}_4]$ can be written as $S = s_a \oplus s_b$. Then we have the following basis vectors as a function of the total spin S, $0 = 1 \oplus 1$ or $0 \oplus 0$, $1 = 1 \oplus 1, 1 \oplus 0$ or $0 \oplus 1$, and $2 = 1 \oplus 1$.

Taking all degrees of freedom of identical particles in the $[Q_1 Q_2]$ ($[\bar{Q}_3 \bar{Q}_4]$) into account, the Pauli principle must be satisfied by imposing restrictions on their quantum numbers to satisfy antisymmetry. The S-wave $[Q_1 Q_2]$ ($[\bar{Q}_3 \bar{Q}_4]$) with two identical quarks (antiquarks) has two possible configurations, $[Q_1 Q_2]_{\bar{\mathbf{3}}_c}^1$ and $[Q_1 Q_2]_{\mathbf{6}_c}^0$ ($[\bar{Q}_3 \bar{Q}_4]_{\mathbf{3}_c}^1$ and $[\bar{Q}_3 \bar{Q}_4]_{\bar{\mathbf{6}}_c}^0$), where the superscript and subscript denote the spin and color representation, respectively. The possible color-flavor-spin functions of the states $[cc][\bar{c}\bar{c}]$, $[bb][\bar{c}\bar{c}]$, and $[bb][\bar{b}\bar{b}]$ states can be written as

$$
\begin{aligned}
0^+: & \; [[Q_1 Q_2]_{\bar{\mathbf{3}}_c}^1 [\bar{Q}_3 \bar{Q}_4]_{\mathbf{3}_c}^1]_{\mathbf{1}_c}^0, \qquad [[Q_1 Q_2]_{\mathbf{6}_c}^0 [\bar{Q}_3 \bar{Q}_4]_{\bar{\mathbf{6}}_c}^0]_{\mathbf{1}_c}^0, \\
1^+: & \; [[Q_1 Q_2]_{\bar{\mathbf{3}}_c}^1 [\bar{Q}_3 \bar{Q}_4]_{\mathbf{3}_c}^1]_{\mathbf{1}_c}^1, \\
2^+: & \; [[Q_1 Q_2]_{\bar{\mathbf{3}}_c}^1 [\bar{Q}_3 \bar{Q}_4]_{\mathbf{3}_c}^1]_{\mathbf{1}_c}^2,
\end{aligned}
$$

those of the states $[cc][\bar{c}\bar{b}]$ and $[bb][\bar{b}\bar{c}]$ read

$$
\begin{aligned}
0^+: & \; [[Q_1 Q_2]_{\bar{\mathbf{3}}_c}^1 [\bar{Q}_3 \bar{Q}_4]_{\mathbf{3}_c}^1]_{\mathbf{1}_c}^0, \qquad [[Q_1 Q_2]_{\mathbf{6}_c}^0 [\bar{Q}_3 \bar{Q}_4]_{\bar{\mathbf{6}}_c}^0]_{\mathbf{1}_c}^0, \\
1^+: & \; [[Q_1 Q_2]_{\bar{\mathbf{3}}_c}^1 [\bar{Q}_3 \bar{Q}_4]_{\mathbf{3}_c}^{0,1}]_{\mathbf{1}_c}^1, \qquad [[Q_1 Q_2]_{\mathbf{6}_c}^0 [\bar{Q}_3 \bar{Q}_4]_{\bar{\mathbf{6}}_c}^1]_{\mathbf{1}_c}^0, \\
2^+: & \; [[Q_1 Q_2]_{\bar{\mathbf{3}}_c}^1 [\bar{Q}_3 \bar{Q}_4]_{\mathbf{3}_c}^1]_{\mathbf{1}_c}^2,
\end{aligned}
$$

those of the state $[cb][\bar{c}\bar{b}]$ read

$$
\begin{aligned}
0^+: & \; [[Q_1 Q_2]_{\bar{\mathbf{3}}_c}^{0,1} [\bar{Q}_3 \bar{Q}_4]_{\mathbf{3}_c}^{0,1}]_{\mathbf{1}_c}^0, \qquad [[Q_1 Q_2]_{\mathbf{6}_c}^{0,1} [\bar{Q}_3 \bar{Q}_4]_{\bar{\mathbf{6}}_c}^{0,1}]_{\mathbf{1}_c}^0, \\
1^+: & \; [[Q_1 Q_2]_{\bar{\mathbf{3}}_c}^{0,1} [\bar{Q}_3 \bar{Q}_4]_{\mathbf{3}_c}^{0,1}]_{\mathbf{1}_c}^1, \qquad [[Q_1 Q_2]_{\mathbf{6}_c}^0 [\bar{Q}_3 \bar{Q}_4]_{\bar{\mathbf{6}}_c}^{0,1}]_{\mathbf{1}_c}^1, \\
2^+: & \; [[Q_1 Q_2]_{\bar{\mathbf{3}}_c}^1 [\bar{Q}_3 \bar{Q}_4]_{\mathbf{3}_c}^1]_{\mathbf{1}_c}^2, \qquad [[Q_1 Q_2]_{\mathbf{6}_c}^1 [\bar{Q}_3 \bar{Q}_4]_{\bar{\mathbf{6}}_c}^1]_{\mathbf{1}_c}^2.
\end{aligned}
$$

In the following, we will extend the three models to study the properties of the states $[Q_1 Q_2][\bar{Q}_3 \bar{Q}_4]$ with the well-defined wave function.

IV. NUMERICAL RESULTS AND DISCUSSIONS

A. Fully-heavy tetraquark states

Recently, various versions of color-magnetic interaction models were widely utilized to investigate the properties of the states $[Q_1 Q_2][\bar{Q}_3 \bar{Q}_4]$. Berezhnoy *et al.* applied a color-magnetic model, in which the tetraquark mass can be determined by solving a two-particle Schrödinger equation with the pointlike diquark (antidiquark) in color $\bar{\mathbf{3}}_c$ ($\mathbf{3}_c$), to research the states $[cc][\bar{c}\bar{c}]$, $[bb][\bar{b}\bar{b}]$ and $[bc][\bar{b}\bar{c}]$. With the exception of the tensor states $[cc][\bar{c}\bar{c}]$ and $[bc][\bar{b}\bar{c}]$, the lowest states with other quantum numbers are all below relevant two meson thresholds [7]. Karliner *et al.* studied the 0^{++} states $[cc][\bar{c}\bar{c}]$ and $[bb][\bar{b}\bar{b}]$ with the color-magnetic interaction model motivated by the QCD-string junction picture [8]. Their masses are, respectively, 6192 ± 25 and 18826 ± 25 MeV. It was noted that an

TABLE IV.   The mass spectra of the ground states $[Q_1Q_2][\bar{Q}_3\bar{Q}_4]$ in the three models, unit in MeV.

Model		CMIM			MCFTM			CQM		
Flavor	J^P	$\bar{3}_c \otimes 3_c$	$6_c \otimes \bar{6}_c$	C.C.	$\bar{3}_c \otimes 3_c$	$6_c \otimes \bar{6}_c$	C.C.	$\bar{3}_c \otimes 3_c$	$6_c \otimes \bar{6}_c$	C.C.
$[cc][\bar{c}\bar{c}]$	0^+	−28.27, 66%	42.40, 34%	−102.64, 6035	6454, 56%	6467, 44%	6407	6573, 36%	6537, 64%	6491
	1^+	0.00, 100%	$\cdots$	0.00, 6139	6463, 100%	$\cdots$	6463	6580, 100%	$\cdots$	6580
	2^+	56.53, 100%	$\cdots$	56.53, 6194	6486, 100%	$\cdots$	6486	6607, 100%	$\cdots$	6607
$[cc][\bar{b}\bar{b}]$	0^+	−13.33, 66%	32.80, 34%	−58.92, 12597	12940, 49%	12938, 51%	12906	13023, 29%	12986, 71%	12963
	1^+	4.27, 100%	$\cdots$	4.27, 12660	12945, 100%	$\cdots$	12945	13024, 100%	$\cdots$	13024
	2^+	39.47, 100%	$\cdots$	39.47, 12695	12960, 100%	$\cdots$	12960	13041, 100%	$\cdots$	13041
$[bb][\bar{b}\bar{b}]$	0^+	−15.47, 66%	23.20, 34%	−56.16, 18834	19377, 38%	19351, 62%	19329	19417, 28%	19368, 72%	19357
	1^+	0.00, 100%	$\cdots$	0.00, 18890	19373, 100%	$\cdots$	19373	19413, 100%	$\cdots$	19413
	2^+	30.93, 100%	$\cdots$	30.93, 18921	19387, 100%	$\cdots$	19387	19429, 100%	$\cdots$	19429
$[cc][\bar{c}\bar{b}]$	0^+	−22.93, 66%	34.40, 34%	−83.27, 9314	9705, 56%	9721, 44%	9670	9813, 41%	9780, 59%	9753
	1^+	−15.85, 65%	16.80, 35%	−53.17, 9343	9705, 58%	9712, 42%	9683	9808, 31%	9785, 69%	9766
	2^+	45.87, 100%	$\cdots$	45.87, 9442	9732, 100%	$\cdots$	9732	9839, 100%	$\cdots$	9839
$[bb][\bar{c}\bar{b}]$	0^+	−16.53, 66%	24.80, 34%	−60.03, 15713	16158, 42%	16158, 58%	16126	16224, 31%	16201, 69%	16175
	1^+	−18.79, 67%	7.20, 33%	−43.33, 15729	16151, 39%	16139, 61%	16130	16230, 23%	16187, 77%	16179
	2^+	33.07, 100%	$\cdots$	33.07, 15806	16182, 100%	$\cdots$	16182	16274, 100%	$\cdots$	16274
$[cb][\bar{c}\bar{b}]$	0^+	−53.24, 33%	−108.10, 67%	−159.37, 12354	12955, 33%	12898, 67%	12829	13043, 29%	12968, 71%	12894
	1^+	−21.81, 28%	−62.04, 72%	−77.75, 12436	12955, 40%	12938, 60%	12881	13052, 33%	13006, 67%	12955
	2^+	34.13, 33%	43.73, 67%	34.13, 12548	12984, 36%	12959, 64%	12925	13084, 27%	13032, 73%	13000

experimental search for these states in the predicted mass range is highly desirable. Wu *et al.* systematically investigated the mass spectra of the states $[Q_1Q_2][\bar{Q}_3\bar{Q}_4]$ with a color-magnetic interaction model with a reference mass scale [9]. It was found that the states $[bb][\bar{b}\bar{c}]$ and $[bc][\bar{b}\bar{c}]$ are possible stable or narrow resonance states.

One should note that all color-magnetic interaction models ignore the spatial degree of freedom so that everything in the models depends only on the color-spin algebra. The generalization of the color-magnetic interaction models from the conventional hadrons to the multiquark states is implemented under the assumption that the spatial configurations of each qq, $q\bar{q}$, and $\bar{q}\bar{q}$ pairs are the same in the multiquark states as in the ordinary hadrons. The well-known H particle predicted in the color-magnetic interaction model was below the $\Lambda\Lambda$ threshold about 80 MeV [26]. However, the state was above the threshold in the nonrelativistic quark model involving the color-magnetic interaction with spatial degree of freedom and other various dynamics once SU(3) flavor symmetry is broken [40]. The state was once very fashionable and searched for in many experiments. The high-sensitivity search at Brookhaven gave no evidence for the production of the state [41]. Recently, the theoretical case for the state continues to be strong and has been strengthened by the NPLQCD and HALQCD collaborations that both observed the state [42,43]. The high-statistics search for the state production shown that no indication of the state with a mass near the $\Lambda\Lambda$ threshold was seen [44].

In view of the inherent defects of the color-magnetic models and the experience of the H particle, it is therefore necessary to make an systematically dynamical investigation on the properties of the states $[Q_1Q_2][\bar{Q}_3\bar{Q}_4]$ in the quark models containing various QCD dynamical effects. The MCFTM and CQM are therefore involved, in which the masses of all possible states $[Q_1Q_2][\bar{Q}_3\bar{Q}_4]$ can be obtained by solving a four-body Schrödinger equation with the well-defined trial wave functions and presented in Table IV. The notations $\bar{3}_c \otimes 3_c$ and $6_c \otimes \bar{6}_c$ stand for the color configurations $[[Q_1Q_2]_{\bar{3}_c}[\bar{Q}_2\bar{Q}_4]_{3_c}]_1$ and $[[Q_1Q_2]_{6_c}[\bar{Q}_3\bar{Q}_4]_{\bar{6}_c}]_1$, respectively. C.C. represents the coupling of the two color configurations. The masses of the states $[Q_1Q_2][\bar{Q}_3\bar{Q}_4]$ with two color configurations and their individual proportion in the eigen states can be achieved by the eigen wave function, which are listed in Table IV. In order to facilitate the comparison, we also reproduce the color-magnetic interaction energy of the states in the CMIM with the approximation $C_{QQ} = C_{Q\bar{Q}}$ [9]. The proportion of each color configuration and the mass (right) obtained with the reference mass formula in the C.C. results are given.

It can be found from Table IV that the masses predicted by the CMIM are lower by 300–500 MeV than those predicted by other two models involving QCD dynamic effects. The masses predicted by the MCFTM are lower 30–120 MeV than those by the CQM. Comparing the masses with the lowest two meson thresholds $T_{M_1M_2}$, the binding energy ΔE in the MCFTM can be calculated and are presented in Table V. One can find that none of states can exist as a bound state because all states are hundreds of MeV above the corresponding threshold in the MCFTM while the masses of the states predicted by the CMIM are close to the corresponding threshold. In order to unveil the

TABLE V. The values of various parts of the Hamiltonian in the MCFTM, unit in MeV.

Flavor	J^P	E_4	$\langle E_k \rangle$	$\langle V_{\min}^{\text{con}}(4) \rangle$	$\langle V^{\text{cm}} \rangle$	$\langle V^{clb} \rangle$	$T_{M_1 M_2}$	ΔE	$\Delta \langle E_k \rangle$	$\Delta \langle V_{\min}^{\text{con}}(4) \rangle$	$\Delta \langle V^{\text{cm}} \rangle$	$\Delta \langle V^{clb} \rangle$
$[cc][\bar{c}\bar{c}]$	0^+	6407	887	192	-51	-1279	$\eta_c \eta_c$	477	-471	42	195	711
	1^+	6463	800	203	4	-1202	$\eta_c \Psi$	395	-367	32	98	632
	2^+	6486	769	211	27	-1178	$\Psi\Psi$	280	-206	18	-31	499
$[cc][\bar{b}\bar{b}]$	0^+	12906	853	131	-27	-1392	$B_c B_c$	418	-435	24	132	696
	1^+	12945	787	135	6	-1324	$B_c^* B_c$	365	-359	17	65	642
	2^+	12960	764	139	20	-1304	$B_c^* B_c^*$	288	-240	9	-20	538
$[bb][\bar{b}\bar{b}]$	0^+	19329	865	69	-26	-1605	$\eta_b \eta_b$	577	-615	21	166	1005
	1^+	19373	826	68	3	-1550	$\eta_b \Upsilon(1S)$	511	-474	14	75	895
	2^+	19387	799	70	17	-1525	$\Upsilon(1S)\Upsilon(1S)$	415	-321	10	-31	756
$[cc][\bar{c}\bar{b}]$	0^+	9670	858	161	-38	-1309	$\eta_c B_c$	461	-465	32	164	730
	1^+	9683	838	165	-25	-1295	$\eta_c B_c^*$	382	-343	25	78	621
	2^+	9732	758	174	22	-1221	ΨB_c^*	293	-232	12	-27	538
$[bb][\bar{c}\bar{b}]$	0^+	16126	856	97	-27	-1483	$B_c \eta_b$	506	-528	19	148	866
	1^+	16130	905	94	-19	-1530	$B_c^* \eta_b$	418	-337	6	58	696
	2^+	16182	771	102	17	-1392	$B_c^* \Upsilon(1S)$	360	-291	8	-27	669
$[cb][\bar{c}\bar{b}]$	0^+	12829	932	123	-84	-1483	$\eta_b \eta_c$	344	-487	24	135	817
	1^+	12881	816	134	-31	-1379	$\eta_c \Upsilon(1S)$	430	-423	29	68	756
	2^+	12925	789	144	21	-1370	$\Psi\Upsilon(1S)$	336	-259	18	-32	608

underlying cause, the average values of various parts in the Hamiltonian are given by using the eigen wave function in Table V, in which $\langle E_k \rangle$, $\langle V^{\text{con}} \rangle$, $\langle V^{\text{cm}} \rangle$ and $\langle V^{clb} \rangle$ represent the average values of kinetic energy, confinement potential, color-magnetic interaction and Coulomb interaction, respectively. The Δ stands for the corresponding interaction difference between the state $[Q_1 Q_2][\bar{Q}_3 \bar{Q}_4]$ and two-meson thresholds. The average distances $\langle \mathbf{r}_{ij}^2 \rangle^{\frac{1}{2}}$ between the particles i and j and $\langle \mathbf{X}^2 \rangle^{\frac{1}{2}}$ between the $[Q_1 Q_2]$ and $[\bar{Q}_3 \bar{Q}_4]$ are presented in Table VI.

The investigation on the spectrum of the heavy mesons in Sec. II indicates that the Coulomb interaction is significant in the formation of the heavy mesons. It can be found from Table V that the interaction also plays a decisive role in the states $[Q_1 Q_2][\bar{Q}_3 \bar{Q}_4]$. The Coulomb interaction provides very strong attraction in the heavy mesons and the states $[Q_1 Q_2][\bar{Q}_3 \bar{Q}_4]$. The interaction depends on $\frac{1}{r}$ and the color factor $\langle \lambda_i^c \cdot \lambda_j^c \rangle$, the strength of which is related to the color factor $\langle \lambda_i^c \cdot \lambda_j^c \rangle$. In the heavy

quark sector, the large quark mass allows two particles to approach each other as a result of a small kinetic, which helps to strengthen the Coulomb interaction. In the heavy mesons, $\langle \lambda_i^c \cdot \lambda_j^c \rangle = -\frac{16}{3}$, which is stronger than those of the states $[Q_1 Q_2][\bar{Q}_3 \bar{Q}_4]$, see Table VII. The states $[Q_1 Q_2][\bar{Q}_3 \bar{Q}_4]$ are therefore looser than heavy mesons η_c, Ψ, B_c, η_b and Υ, see the average distances in Tables III and VI. In addition, the values of the Coulomb interaction in the states $[Q_1 Q_2][\bar{Q}_3 \bar{Q}_4]$ are higher by 500–1000 MeV than those of their corresponding two-meson thresholds, see the difference $\Delta \langle V^{clb} \rangle$ in Table V, which is the main reason resulting in none of bound states in the quark models with QCD dynamic effects. It is therefore difficult for the CMIM to completely absorb the strong Coulomb interaction effect in the states $[Q_1 Q_2][\bar{Q}_3 \bar{Q}_4]$ by the effective constituent quark mass.

The long-range confinement interaction contributes a little to the masses and binding energy of the ground states $[Q_1 Q_2][\bar{Q}_3 \bar{Q}_4]$ because of the small distances, see the

TABLE VI. The average distances $\langle \mathbf{r}_{ij}^2 \rangle^{\frac{1}{2}}$ and $\langle \mathbf{X}^2 \rangle^{\frac{1}{2}}$ of the ground states $[Q_1 Q_2][\bar{Q}_3 \bar{Q}_4]$ in the MCFTM, unit in fm.

State	$[cc][\bar{c}\bar{c}]$			$[cc][\bar{b}\bar{b}]$			$[bb][\bar{b}\bar{b}]$			$[cc][\bar{c}\bar{b}]$			$[bb][\bar{c}\bar{b}]$			$[bc][\bar{b}\bar{c}]$		
J^P	0^+	1^+	2^+	0^+	1^+	2^+	0^+	1^+	2^+	0^+	1^+	2^+	0^+	1^+	2^+	0^+	1^+	2^+
$\langle \mathbf{r}_{12}^2 \rangle^{\frac{1}{2}}$	0.44	0.44	0.44	0.42	0.42	0.42	0.27	0.25	0.26	0.43	0.43	0.43	0.28	0.28	0.27	0.37	0.38	0.40
$\langle \mathbf{r}_{34}^2 \rangle^{\frac{1}{2}}$	0.44	0.44	0.44	0.30	0.28	0.28	0.27	0.25	0.26	0.38	0.38	0.38	0.35	0.35	0.35	0.37	0.38	0.40
$\langle \mathbf{r}_{13}^2 \rangle^{\frac{1}{2}}$	0.44	0.47	0.48	0.36	0.39	0.39	0.26	0.27	0.28	0.45	0.46	0.48	0.36	0.36	0.38	0.24	0.26	0.26
$\langle \mathbf{r}_{24}^2 \rangle^{\frac{1}{2}}$	0.44	0.47	0.48	0.36	0.39	0.39	0.26	0.27	0.28	0.36	0.37	0.40	0.26	0.26	0.29	0.44	0.46	0.47
$\langle \mathbf{r}_{14}^2 \rangle^{\frac{1}{2}}$	0.44	0.47	0.48	0.36	0.39	0.39	0.26	0.27	0.28	0.36	0.37	0.40	0.26	0.26	0.29	0.35	0.37	0.38
$\langle \mathbf{r}_{23}^2 \rangle^{\frac{1}{2}}$	0.44	0.47	0.48	0.36	0.39	0.39	0.26	0.27	0.28	0.45	0.46	0.48	0.36	0.36	0.38	0.35	0.37	0.38
$\langle \mathbf{X}^2 \rangle^{\frac{1}{2}}$	0.31	0.36	0.37	0.25	0.29	0.30	0.17	0.20	0.21	0.28	0.29	0.33	0.20	0.20	0.24	0.20	0.22	0.22

TABLE VII. Color matrix elements, $\hat{O}_{ij} = \lambda_i^c \cdot \lambda_j^c$.

$\langle\hat{O}_{ij}\rangle$	$\langle\hat{O}_{12}\rangle$	$\langle\hat{O}_{34}\rangle$	$\langle\hat{O}_{13}\rangle$	$\langle\hat{O}_{24}\rangle$	$\langle\hat{O}_{14}\rangle$	$\langle\hat{O}_{23}\rangle$
$\langle\bar{3}_c \otimes 3_c\|\hat{O}_{ij}\|\bar{3}_c \otimes 3_c\rangle$	$-\frac{8}{3}$	$-\frac{8}{3}$	$-\frac{4}{3}$	$-\frac{4}{3}$	$-\frac{4}{3}$	$-\frac{4}{3}$
$\langle 6_c \otimes \bar{6}_c\|\hat{O}_{ij}\|6_c \otimes \bar{6}_c\rangle$	$\frac{4}{3}$	$\frac{4}{3}$	$-\frac{10}{3}$	$-\frac{10}{3}$	$-\frac{10}{3}$	$-\frac{10}{3}$
$\langle\bar{3}_c \otimes 3_c\|\hat{O}_{ij}\|6_c \otimes \bar{6}_c\rangle$	0	0	$-2\sqrt{2}$	$-2\sqrt{2}$	$2\sqrt{2}$	$2\sqrt{2}$

average values $V_{\min}^{\mathrm{con}}$ and $\Delta V_{\min}^{\mathrm{con}}$ in Table V. The mass difference, about 30–120 MeV, between the CQM and MCFTM in Table IV originates from different types of confinement potential. The multibody confinement potential based on the lattice color flux-tube picture is thought to be closer to real physical images than two-body one related to color charges, which plays significant roles in many interesting places of hadron physics, such as the formation and decay of the multiquark states via strong interaction, quark pair creation and hadron structure. The multibody confinement potential can reduce the mass of the multiquark states. Similar quark models with different type of multibody confinement potential have been extensively applied to study the properties of the multiquark states [45].

The CMIM does not explicitly involve the spatial degree of freedom, which in fact implies that any two pairs of interacting particles with the same quark content have the same spatial configuration in despite of hadron environments, such as the $Q\bar{Q}$ in the conventional mesons and multiquark states. The dynamical calculations on the heavy mesons and the states $[Q_1Q_2][\bar{Q}_3\bar{Q}_4]$ indicate that the difference of their distances are apparent, see Tables III and VI, which is in contradiction with the CMIM assumption of the same spatial configuration. Furthermore, it can be found from Tables IV and V that the color-magnetic interactions of the states $[Q_1Q_2][\bar{Q}_3\bar{Q}_4]$ in the CMIM are overestimated relative to that in the dynamical models due to the spatial assumption, which results in the appearance of the bound states in the CMIM [9]. In addition, the difference of the confinement potential based on string and junction $\Delta\langle V_{\min}^{\mathrm{con}}(4)\rangle$ is not a constant, which depends on the specific state. However, the added constant term S may be thought of as representing the contribution of two additional QCD strings and one junction [8]. In this way, the predictive power of the color-magnetic mechanism needs to be checked on a large scale by more sophisticated models with various QCD dynamic effects.

The ground states $[Q_1Q_2][\bar{Q}_3\bar{Q}_4]$ prefer the color configuration $\bar{3}_c \otimes 3_c$ in the color-magnetic mechanism [7,8]. However, the interactions between the $[Q_1Q_2]_{6_c}$ and $[\bar{Q}_3\bar{Q}_4]_{\bar{6}}$ in the color configuration $6_c \otimes \bar{6}_c$ are attractive although the interactions in the $[Q_1Q_2]_{6_c}$ ($[\bar{Q}_3\bar{Q}_4]_{6}$) are repulsive. The attractive interactions are much stronger than those of the $\bar{3}_c \otimes 3_c$ because the strength of the interaction depends on the color factors listed in Table VII. Therefore,

the final result, which is mainly dominated by the Coulomb interaction, of the $6_c \otimes \bar{6}_c$ relies on the distance $\langle\mathbf{X}^2\rangle^{\frac{1}{2}}$ between the $[Q_1Q_2]_{6_c}$ and $[\bar{Q}_3\bar{Q}_4]_{\bar{6}}$. The heavier the heavy quark mass, the smaller the distance $\langle\mathbf{X}^2\rangle^{\frac{1}{2}}$, the stronger the Coulomb interaction, the bigger the proportion of the $6_c \otimes \bar{6}_c$, which can be found from the group $[cc][\bar{c}\bar{c}] - [cc][\bar{b}\bar{b}] - [bb][\bar{b}\bar{b}]$ with 0^+ in Tables V and VI.

The $\bar{3}_c \otimes 3_c$ and $6_c \otimes \bar{6}_c$ can couple each other through mainly the color-magnetic interaction, the strength of which is inversely proportional to the interacting quark masses. The proportion of the $6_c \otimes \bar{6}_c$ in the CQM is bigger than that in the MCFTM because the confinement potential involving the color factor $\langle\lambda_i^c \cdot \lambda_j^c\rangle$ in the CQM can strengthen the coupling in the two color configurations, see Table IV. In the CMIM, the proportion in the group $[cc][\bar{c}\bar{c}] - [cc][\bar{b}\bar{b}] - [bb][\bar{b}\bar{b}]$ with 0^+ in Tables V does not change because it only determined by spin-color structure due to the absence of the spatial degree of freedom. In a word, the color configuration $6_c \otimes \bar{6}_c$ can not be ignored but should be taken seriously in the investigation on the ground fully-heavy tetraquark states, which is supported by the conclusions of other two models with QCD dynamical effects [4].

The $[Q_1Q_2]$ and $[\bar{Q}_3\bar{Q}_4]$ are both considered as a compound object with no internal orbital excitations, namely $l_a = l_b = 0$. In the case of the excited states $[Q_1Q_2][\bar{Q}_3\bar{Q}_4]$, the orbital angular excitations are assumed to occur only between the $[Q_1Q_2]$ and $[\bar{Q}_3\bar{Q}_4]$ in the present numerical calculations. Therefore, the total orbital angular momentum of the states $[Q_1Q_2][\bar{Q}_3\bar{Q}_4]$ L is equal to l_{ab} and the parity is $P = (-1)^L$. In Table VIII, we present the numerical results of the states $[cc][\bar{c}\bar{c}]$, $[cc][\bar{b}\bar{b}]$, and $[bb][\bar{b}\bar{b}]$ with $L = 0$, 1, and 2 and $S = 0$. It can be found from Tables VI and VIII that the sizes of the $[Q_1Q_2]$ and $[\bar{Q}_3\bar{Q}_4]$, $\langle\mathbf{r}_{12}^2\rangle^{\frac{1}{2}}$ and $\langle\mathbf{r}_{34}^2\rangle^{\frac{1}{2}}$, do not dramatically change with the increase of L and S. However, the distance between the $[Q_1Q_2]$ and $[\bar{Q}_3\bar{Q}_4]$ $\langle\mathbf{X}^2\rangle^{\frac{1}{2}}$ rapidly increase with the increase of L in the excited states. It can be concluded form the average distances that the spatial configuration of the states $[Q_1Q_2][\bar{Q}_3\bar{Q}_4]$ is a compact three-dimensional structure. In the ground states ($L = 0$), the shape looks like an ellipsoid because the $[Q_1Q_2]$ and $[\bar{Q}_3\bar{Q}_4]$ overlap very strongly. In the excited states, the ellipsoid gradually expands to be a dumbbell-like shape with the increase of the distance $\langle\mathbf{X}^2\rangle^{\frac{1}{2}}$ because of the increase of L.

The Coulomb interaction between the $[Q_1Q_2]$ and $[\bar{Q}_3\bar{Q}_4]$ rapidly decrease with the increase of the distance $\langle\mathbf{X}^2\rangle^{\frac{1}{2}}$. The $6_c \otimes \bar{6}_c$ decreases faster than the $\bar{3}_c \otimes 3_c$ because of the bigger interaction strength between the $[Q_1Q_2]_{6_c}$ and $[\bar{Q}_3\bar{Q}_4]_{\bar{6}}$. The Coulomb interaction in the $\bar{3}_c \otimes 3_c$ is stronger than that in the $6_c \otimes \bar{6}_c$ because the Coulomb interaction in the $[Q_1Q_2]_{\bar{3}}$ and $[\bar{Q}_3\bar{Q}_4]_{3}$ is

TABLE VIII. The average values of various parts of the Hamiltonian in MeV, the average distances in fm of the states $[cc][\bar{c}\bar{c}]$, $[cc][\bar{b}\bar{b}]$, and $[bb][\bar{b}\bar{b}]$ in the MCFTM.

	LS	J^P	States	Mass, prop.	$\langle E_k\rangle$	$\langle V_{min}^{com}(4)\rangle$	$\langle V^{cm}\rangle$	$\langle V^{clb}\rangle$	$\langle r_{12}^2\rangle^{\frac{1}{2}}$	$\langle r_{34}^2\rangle^{\frac{1}{2}}$	$\langle r_{13}^2\rangle^{\frac{1}{2}}$	$\langle r_{24}^2\rangle^{\frac{1}{2}}$	$\langle r_{14}^2\rangle^{\frac{1}{2}}$	$\langle r_{23}^2\rangle^{\frac{1}{2}}$	$\langle X^2\rangle^{\frac{1}{2}}$
$[cc][\bar{c}\bar{c}]$	00	0^+	$\bar{3}_c\otimes 3_c$	6454, 56%	878	188	−11	−1258	0.42	0.42	0.45	0.45	0.45	0.45	0.33
			$6_c\otimes\bar{6}_c$	6467, 44%	899	199	17	−1306	0.46	0.46	0.43	0.43	0.43	0.43	0.28
			C.C.	6407	887	192	−51	−1279	0.44	0.44	0.44	0.44	0.44	0.44	0.31
	10	1^-	$\bar{3}_c\otimes 3_c$	6730, 98%	783	283	4	−997	0.47	0.47	0.61	0.61	0.61	0.61	0.52
			$6_c\otimes\bar{6}_c$	6888, 2%	910	274	12	−966	0.51	0.51	0.54	0.54	0.54	0.54	0.40
			C.C.	6727	785	283	−2	−997	0.47	0.47	0.61	0.61	0.61	0.61	0.51
	20	2^+	$\bar{3}_c\otimes 3_c$	6995, > 99%	802	364	9	−888	0.48	0.48	0.75	0.75	0.75	0.75	0.66
			$6_c\otimes\bar{6}_c$	7213, < 1%	978	339	10	−772	0.55	0.55	0.63	0.63	0.63	0.63	0.50
			C.C.	6944	802	364	8	−887	0.48	0.48	0.75	0.75	0.75	0.75	0.66
$[bb][\bar{c}\bar{c}]$	00	0^+	$\bar{3}_c\otimes 3_c$	12939, 41%	847	127	−3	−1372	0.27	0.41	0.37	0.37	0.37	0.37	0.29
			$6_c\otimes\bar{6}_c$	12938, 51%	859	135	13	−1411	0.33	0.42	0.35	0.35	0.35	0.35	0.23
			C.C.	12906	853	131	−27	−1392	0.30	0.42	0.36	0.36	0.36	0.36	0.25
	10	1^-	$\bar{3}_c\otimes 3_c$	13204, > 99%	727	201	6	−1071	0.30	0.46	0.52	0.52	0.52	0.52	0.45
			$6_c\otimes\bar{6}_c$	13370, < 1%	884	186	9	−1051	0.36	0.48	0.44	0.44	0.44	0.44	0.32
			C.C.	13204	728	201	4	−1071	0.30	0.46	0.52	0.52	0.52	0.52	0.45
	20	2^+	$\bar{3}_c\otimes 3_c$	13398, > 99%	727	267	8	−946	0.31	0.48	0.65	0.65	0.65	0.65	0.58
			$6_c\otimes\bar{6}_c$	13696, < 1%	954	235	7	−842	0.36	0.53	0.52	0.52	0.52	0.52	0.40
			C.C.	13398	727	267	8	−946	0.31	0.48	0.65	0.65	0.65	0.65	0.58
$[bb][\bar{b}\bar{b}]$	00	0^+	$\bar{3}_c\otimes 3_c$	19367, 38%	899	63	−6	−1615	0.24	0.24	0.26	0.26	0.26	0.26	0.19
			$6_c\otimes\bar{6}_c$	19352, 62%	884	72	9	−1638	0.28	0.28	0.25	0.25	0.25	0.25	0.16
			C.C.	19329	865	69	−26	−1605	0.27	0.27	0.26	0.26	0.26	0.26	0.17
	10	1^-	$\bar{3}_c\otimes 3_c$	19636, > 99%	700	110	4	−1204	0.29	0.29	0.39	0.39	0.39	0.39	0.33
			$6_c\otimes\bar{6}_c$	19792, < 1%	854	104	6	−1198	0.32	0.32	0.32	0.32	0.32	0.32	0.23
			C.C.	19635	701	110	2	−1204	0.29	0.29	0.39	0.39	0.39	0.39	0.33
	20	2^+	$\bar{3}_c\otimes 3_c$	19812, > 99%	659	157	6	−1035	0.31	0.31	0.50	0.50	0.50	0.50	0.45
			$6_c\otimes\bar{6}_c$	20105, < 1%	898	136	4	−960	0.36	0.36	0.39	0.39	0.39	0.39	0.29
			C.C.	19812	659	157	6	−1035	0.31	0.31	0.50	0.50	0.50	0.50	0.45

strongly attractive while that in the $[Q_1Q_2]_{6_c}$ and $[\bar{Q}_3\bar{Q}_4]_{\bar{6}}$ is repulsive. In addition, the kinetic E_k of the $\bar{3}_c\otimes 3_c$ is obviously lower, more than 100 MeV, than that of the $6_c\otimes\bar{6}_c$ because of the big distance $\langle X^2\rangle^{\frac{1}{2}}$ induced by the relative weak Coulomb interaction between the $[Q_1Q_2]_{\bar{3}}$ and $[\bar{Q}_3\bar{Q}_4]_3$, see Table VIII, which is the main reason resulting in the mass difference between the $\bar{3}_c\otimes 3_c$ and $6_c\otimes\bar{6}_c$. The coupling effect between the $\bar{3}_c\otimes 3_c$ and $6_c\otimes\bar{6}_c$ is very weak because of the weak color-magnetic interaction in the excited states. In this way, the proportion of the $6_c\otimes\bar{6}_c$ is small in the excited states while the $\bar{3}_c\otimes 3_c$ is absolutely dominant.

Other different versions of nonrelativistic quark models involving the OGE interaction and various type of color confinement potential were also employed to investigate the fully-heavy tetraquark states [3–5], which presented similar mass spectra to our models. The masses of the ground states in those quark models are much higher, about 300–500 MeV, than the corresponding thresholds, which indicates that there does not exist a bound state in the scheme of those quark models. However, the nonrelativistic model with a Cornell-inspired potential, in which a four-body problem is simplified into three two-body problems, predicted that the lowest S-wave $[cc][\bar{c}\bar{c}]$ might be below their thresholds of spontaneous dissociation into low-lying charmonium pairs [46].

B. J/Ψ-pair resonances observed by LHCb and the fully-heavy state $[cc][\bar{c}\bar{c}]$

The central value of the broad structure ranging from 6.2 to 6.8 GeV locates at around 6490 MeV [18]. The mass and width of the structure $X(6900)$ are

$$M = 6905 \pm 11 \pm 7 \text{ MeV}, \qquad \Gamma = 80 \pm 19 \pm 33 \text{ MeV}$$

assuming no interference with the nonresonant single-parton scattering continuum [18]. The mass and width are changed to

$$M = 6886 \pm 11 \pm 11 \text{ MeV}, \quad \Gamma = 168 \pm 33 \pm 69 \text{ MeV}$$

when assuming the nonresonant single-parton scattering continuum interferes with the broad structure [18]. The two structures are obviously higher than the CMIM predictions

TABLE IX. Masses of the ground state $[cc][\bar{c}\bar{c}]$ in various models, unit in MeV.

J^P	MCFTM	CQM	[3]	I, II [4]	[5]	[20]	[47]
0^+	6407	6491	6477	6377, 6371	6470	6350	6440 ± 0.15
1^+	6463	6580	6528	6425, 6450	6512	6440	6370 ± 0.18
2^+	6486	6607	6573	6432, 6479	6534	6470	6370 ± 0.19

on the state $[cc][\bar{c}\bar{c}]$, see Table IV. In this way, the two structures are difficult to be accommodated in the CMIM.

The mass of the ground state $[cc][\bar{c}\bar{c}]$ ranges from 6370 to 6600 MeV in the MCFTM, CQM and other non-relativistic quark models with various dynamical effects [3–5,20], see Table IX, which is supported by QCD sum rule [47]. Matching the central value of the broad structure ranging from 6.2 to 6.8 GeV with the model results, the structure can be described as the ground state $[cc][\bar{c}\bar{c}]$ in the models. However, the models give different quantum numbers. In the MCFTM and the model II in the literature [4], the ground states $[cc][\bar{c}\bar{c}]$ with 1^+ and 2^+ are both close to the central value. The masses of the ground state $[cc][\bar{c}\bar{c}]$ with 0^+, 1^+, and 2^+ are very close to each other, around 6500 MeV, in the model in the literature [5]. In the CQM, the ground state $[cc][\bar{c}\bar{c}]$ with 0^+ has a mass of 6491 MeV, which is very consistent with the value. In the model in the literature [20], the mass of the ground tetraquark state $[cc][\bar{c}\bar{c}]$ with 2^+ is closest to the central value. The matching inconsistence results from the slight difference of the model dynamics.

The masses of the excited state $[cc][\bar{c}\bar{c}]$ with $L = 1$, 2 and $S = 0$, 1, 2 are calculated in the MCFTM and CQM, which are given in Table X. The spin-orbital interaction is not taken into account in the present calculation because it is very weak, about several MeV [23]. One can find that the effect of the spin-dependent interaction on the masses of the excited state with different total spin is small. The masses in the CQM are apparent higher than those in the MCFTM, about 175 MeV for the excited states with $L = 1$ and about 240 MeV for the excited states with $L = 2$, which originates from the different forms of confinement potential. In the CQM, the masses of the excited state $[cc][\bar{c}\bar{c}]$ with $L = 1$ are completely consistent with that of the narrow structure $X(6900)$. Therefore, the structure can be described as the excited state $[cc][\bar{c}\bar{c}]$ with $L = 1$ in the CQM, which is supported by the NRPQM [48]. However,

TABLE X. Masses of the excited state $[cc][\bar{c}\bar{c}]$ in the CQM and MCFTM, unit in MeV.

L		1			2	
S	0	1	2	0	1	2
CQM	6901	6912	6924	7182	7185	7191
MCFTM	6727	6735	6744	6944	6947	6951

the masses of the excited states $[cc][\bar{c}\bar{c}]$ with $L = 1$ in the MCFTM are obviously lower than that of the narrow structure, while the excited states $[cc][\bar{c}\bar{c}]$ with $L = 2$ are very close to the narrow structure.

V. SUMMARY

In this work, we use the CMIM and two quark models with the OGE interaction and color confinement potential, CQM with two-body confinement and MCFTM with multibody one based on the lattice color flux-tube picture, to systematically investigate the properties of the states $[Q_1 Q_2][\bar{Q}_3 \bar{Q}_4]$. The difference between the two confinement potentials in the ground states is 30–120 MeV. In the excited states with $L \leq 2$, the difference is around 200 MeV.

The masses of the ground states $[Q_1 Q_2][\bar{Q}_3 \bar{Q}_4]$ predicted by the CMIM are close to the corresponding two heavy-meson threshold, which is much lower, about hundreds of MeV, than the masses predicted by the models with QCD dynamic effects mainly because of the strong Coulomb interaction. Therefore, the CMIM can not completely absorb QCD dynamic effects. In addition, the CMIM may overestimate the color-magnetic interaction in the extension from heavy mesons to the states $[Q_1 Q_2] \times [\bar{Q}_3 \bar{Q}_4]$ because of the assumption of the same spatial configurations. Therefore, the reliability of the CMIM extension from the conventional hadrons to multiquark states needs further study.

The Coulomb interaction plays an important role in the dynamical model calculation on the heavy mesons. The interaction in the states $[Q_1 Q_2][\bar{Q}_3 \bar{Q}_4]$ is weaker than that of the corresponding threshold of two heavy meons, which directly induces the fact that there does not exist a bound state $[Q_1 Q_2][\bar{Q}_3 \bar{Q}_4]$ in the dynamical models. The color configuration $[[Q_1 Q_2]_{6_c}[\bar{Q}_3 \bar{Q}_4]_{\bar{6}_c}]_1$ can not be ignored in the ground states owing to the strong Coulomb interaction between the $[Q_1 Q_2]_{6_c}$ and $[\bar{Q}_3 \bar{Q}_4]_{\bar{6}_c}$ at the short distance. The color configuration $[[Q_1 Q_2]_{\bar{3}_c}[\bar{Q}_2 \bar{Q}_4]_{3_c}]_1$ is absolutely dominant in the excited states because the Coulomb interaction in the $[Q_1 Q_2]_{\bar{3}}$ and $[\bar{Q}_3 \bar{Q}_4]_3$ is strongly attractive, while that in the $[Q_1 Q_2]_{6_c}$ and $[\bar{Q}_3 \bar{Q}_4]_{\bar{6}}$ is repulsive.

The J/Ψ-pair resonances observed by LHCb are difficult to be accommodated in the CMIM because their masses are much higher than the CMIM predictions on the state $[cc][\bar{c}\bar{c}]$. The broad structure ranging from 6.2 to 6.8 GeV can be described as the ground tetraquark state $[cc][\bar{c}\bar{c}]$ in the various quark models. However, it has different quantum numbers because of the slight difference of the dynamics in the models. The narrow structure $X(6900)$ can be described as the excited state $[cc][\bar{c}\bar{c}]$ with $L = 1$ in the CQM. However, the masses of the states $[cc][\bar{c}\bar{c}]$ with $L = 2$ in the MCFTM are very close to that of the narrow structure. Although many theoretical

investigations have been devoted to those structures, the interpretations on the natures of the two structure are not completely consistent in the different theoretical frames so far. Therefore, more data along with additional measurements, including determination of the spin-parity quantum numbers, are needed, which will contribute immeasurably to an understanding of the properties of these structures.

[1] Y. Iwasaki, Prog. Theor. Phys. **54,** 492 (1975).
[2] S. Zouzou, B. Silvestre-Brac, C. Gignoux, and J. M. Richard, Z. Phys. C **30,** 457 (1986); N. Barnea, J. Vijande, and A. Valcarce, Phys. Rev. D **73,** 054004 (2006).
[3] R. J. Lloyd and J. P. Vary, Phys. Rev. D **70,** 014009 (2004).
[4] G. J. Wang, L. Meng, and S. L. Zhu, Phys. Rev. D **100,** 096013 (2019).
[5] M. S. Liu, Q. F. Lü, X. H. Zhong, and Q. Zhao, Phys. Rev. D **100,** 016006 (2019).
[6] B. Silvestre-Brac, Phys. Rev. D **46,** 2179 (1992).
[7] A. V. Berezhnoy, A. K. Likhoded, A. V. Luchinsky, and A. A. Novoselov, Phys. Rev. D **84,** 094023 (2011); A. V. Berezhnoy, A. V. Luchinsky, and A. A. Novoselov, Phys. Rev. D **86,** 034004 (2012).
[8] M. Karliner, S. Nussinov, and J. L. Rosner, Phys. Rev. D **95,** 034011 (2017).
[9] J. Wu, Y. R. Liu, K. Chen, X. Liu, and S. L. Zhu, Phys. Rev. D **97,** 094015 (2018).
[10] W. Chen, H. X. Chen, X. Liu, T. G. Steele, and S. L. Zhu, Phys. Lett. B **773,** 247 (2017); Z. G. Wang, Eur. Phys. J. C **77,** 432 (2017); Z. G. Wang and Z. Y. Di, Acta Phys. Pol. B **50,** 1335 (2019).
[11] W. Heupel, G. Eichmann, and C. S. Fischer, Phys. Lett. B **718,** 545 (2012).
[12] J. P. Ader, J.-M. Richard, and P. Taxil, Phys. Rev. D **25,** 2370 (1982); H. J. Lipkin, Phys. Lett. B **172,** 242 (1986); L. Heller and J. A. Tjon, Phys. Rev. D **32,** 755 (1985).
[13] C. Hughes, E. Eichten, and Christine T. H. Davies, Phys. Rev. D **97,** 054505 (2018).
[14] A. Esposito and A. D. Polosa, Eur. Phys. J. C **78,** 782 (2018).
[15] J. M. Richard, A. Valcarce, and J. Vijande, Phys. Rev. D **95,** 054019 (2017).
[16] R. Aaij *et al.*, Phys. Lett. B **707,** 52 (2012); M. Aaboud *et al.*, Eur. Phys. J. C **77,** 76 (2017).
[17] R. Aaij *et al.* (LHCb Collaboration), J. High Energy Phys. 10 (2018) 086.
[18] R. Aaij *et al.* (LHCb Collaboration), Sci. Bull. **65,** 1983 (2020).
[19] C. Becchi, A. Giachino, L. Maiani, and E. Santopinto, arXiv:2006.14388; G. Yang, J. L. Ping, L. Y. He, and Q. Wang, arXiv:2006.13756; H. X. Chen, W. Chen, X. Liu, and S. L. Zhu, Sci. Bull. **65,** 1994 (2020); J. Sonnenschein and D. Weissman, arXiv:2008.01095; J. F. Giron and R. F. Lebed, Phys. Rev. D **102,** 074003 (2020); L. Maiani,

arXiv:2008.01637; J. M. Richard, arXiv:2008.01962; J. Z. Wang, D. Y. Chen, X. Liu, and T. Matsuki, arXiv:2008.07430; K. T. Chao and S. L. Zhu, Sci. Bul. **65,** 1952 (2020); R. Maciuła, W. Schäfer, and A. Szczurek, arXiv:2009.02100.
[20] M. C. Gordillo, F. De Soto, and J. Segovia, arXiv:2009.11889v1.
[21] Y. R. Liu, H. X. Chen, W. Chen, X. Liu, and S. L. Zhu, Prog. Part. Nucl. Phys. **107,** 237 (2019).
[22] J. Wu, Y. R. Liu, K. Chen, X. Liu, and S. L. Zhu, Phys. Rev. D **95,** 034002 (2017); J. Wu, Y. R. Liu, K. Chen, X. Liu, and S. L. Zhu, Phys. Rev. D **97,** 094015 (2018); Q. S. Zhou, K. Chen, X. Liu, Y. R. Liu, and S. L. Zhu, Phys. Rev. C **98,** 045204 (2018).
[23] C. R. Deng, H. Chen, and J. L. Ping, Phys. Rev. D **101,** 054039 (2020).
[24] A. De Rujula, H. Georgi, and S. L. Glashow, Phys. Rev. D **12,** 147 (1975).
[25] J. Vijande and A. Valcarce, Symmetry **1,** 155 (2009).
[26] R. L. Jaffe, Phys. Rev. Lett. **38,** 195 (1977).
[27] C. Gignoux, B. Silvestre-Brac, and J.-M. Richard, Phys. Lett. B **193,** 323 (1987); H. J. Lipkin, Phys. Lett. B **195,** 484 (1987).
[28] J. Wu, Y. R. Liu, K. Chen, X. Liu, and S. L. Zhu, Phys. Rev. D **94,** 094031 (2016); K. Chen, X. Liu, J. Wu, Y. R. Liu, and Shi-Lin Zhu, Eur. Phys. J. A **53,** 5 (2017); S. Y. Li, Y. R. Liu, Y. N. Liu, Z. G. Si, and J. Wu, Eur. Phys. J. C **79,** 87 (2019).
[29] F. Stancu, J. Phys. G **37,** 075017 (2010).
[30] J. Leandri and B. Silvestre-Brac, Phys. Rev. D **40,** 2340 (1989); B. Silvestre-Brac and J. Leandri, Phys. Rev. D **45,** 4221 (1992).
[31] R. K. Bhaduri, L. E. Cohler, and Y. Nogami, Phys. Rev. Lett. **44,** 1369 (1980).
[32] J. Vijande, F. Fernandez, and A. Valcarce, J. Phys. G **31,** 481 (2005).
[33] J. Weinstein and N. Isgur, Phys. Rev. D **27,** 588 (1983).
[34] G. M. Prosperi, M. Raciti, and C. Simolo, Prog. Part. Nucl. Phys. **58,** 387 (2007).
[35] J. Weinstein and N. Isgur, Phys. Rev. D **27,** 588 (1983).
[36] J. Weinstein and N. Isgur, Phys. Rev. D **41,** 2236 (1990).
[37] V. Dmitrasinovic, Phys. Rev. D **67,** 114007 (2003).
[38] E. Hiyama, Y. Kino, and M. Kamimura, Prog. Part. Nucl. Phys. **51,** 223 (2003).

[39] G. S. Bali, Phys. Rev. D **62**, 114503 (2000); C. Semay, Eur. Phys. J. A **22**, 353 (2004); N. Cardoso, M. Cardoso, and P. Bicudo, Phys. Lett. B **710**, 343 (2012).

[40] B. Silvestre-Brac, J. Carbonell, and C. Gignoux, Phys. Rev. D **36**, 2083 (1987); M. Oka, K. Shimizu, and K. Yazaki, Phys. Lett. B **130**, 365 (1983).

[41] R. W. Stotzer, T. Burger, P. D. Barnes, B. Bassalleck, A. R. Berdoz, and M. Burger *et al.*, Phys. Rev. Lett. **78**, 3646 (1997).

[42] S. R. Beane *et al.* (NPLQCD Collaboration), Phys. Rev. Lett. **106**, 162001 (2011).

[43] T. Inoue, N. Ishii, S. Aoki, T. Doi, T. Hatsuda, Y. Ikeda, K. Murano, H. Nemura, and K. Sasaki (HALQCD Collaboration), Phys. Rev. Lett. **106**, 162002 (2011).

[44] B. H. Kim *et al.* (Belle Collaboration), Phys. Rev. Lett. **110**, 222002 (2013).

[45] J. M. Richard, A. Valcarce, and J. Vijande, Phys. Rev. D **95**, 054019 (2017); J. Vijande, A. Valcarce, and J. M. Richard, Phys. Rev. D **85**, 014019 (2012); M. Cardoso, N. Cardoso, and P. Bicudo, Phys. Rev. D **86**, 014503 (2012); N. Cardoso and P. Bicudo, Phys. Rev. D **87**, 034504 (2013).

[46] V. R. Debastiani and F. S. Navarra, Chin. Phys. C **43**, 013105 (2019).

[47] W. Chen, H. X. Chenb, X. Liu, T. G. Steelea, and S. L. Zhu, Phys. Lett. B **773**, 247 (2017).

[48] M. S. Liu, F. X. Liu, X. H. Zhong, and Q. Zhao, arXiv:2006.11952.